ANALYSIS AND SIMULATION OF CALENDERING PROCESS OF NON-NEWTONIAN POLYMERIC FLUIDS

Jeong Su Yu, Jae Wook Lee* and Ki Jun Lee**

Department of Chemical Engineering, Seoul National University, Seoul 151, Korea
* Department of Chemical Engineering, Sogang University, Seoul

(Received 11 June 1984• accepted 24 July 1984)

Abstract—Maxwellian fluid flow between asymmetric calenders was analyzed by the numerical solution to the simplified equations of motion and energy equation. The solution techniques combined the power-law weighted upwind difference method for the energy equation with the analytical solution of the momentum equations. The calculated results provided not only pressure and temperature distributions of the flow field, but also the power consumption and the roll separating force of the calendering processes. The decrease in the elastic shear modulus led to the reduction in the temperature profile as well as in the power requirement. The asymmetry in the roll speeds generated higher temperature field throughout the whole flow region due to the higher viscous heating, compared with the case of the symmetry in the roll speeds.

INTRODUCTION

Calendering process is commonly used for shaping films of thermoplastic materials and is particularly suitable for polymers succeptible to thermal degradation. This is usually accomplished by a pair of heated driven rolls with equal or unequal diameters in a 'Z' or 'inverse L' arrangement.

The early hydrodynamic theory of calendering was developed by Gaskell [1]. The validity of his model was confirmed by the experimental measurement of pressure distribution perfomred by Bergen and Scott [2].

Following the Gaskell's model, a great deal of effort was invested to the theoretical analysis on the calendering processes by numerous workers. Most of these efforts concentrated on dealing basically with more realistic constitutive equations and attempted to account for nonisothermal effects. Mckelvey [3], Brazinsky et al. [4] and Torner [5] discussed the power-law fluid, while Alston and Astill [6] treated a hyperbolic tangent model. Paslay [7] obtained an approximate solution essentially based on the Maxwell fluid for the Weissenberg number smaller than unity. The results of his numerical solution indicated that the pressure and the shear stress dropped as the elastic shear modulus was lowered. Tokita and White [8] related the experimental results on milling of elastomers to rheological parameters of the second order Rivlin-Ericksen fluid. Chong [9] found by experiment that the Weissenberg number was an important parameter in determining the onset of a nonuniform internal strain pattern.

The problems of the asymmetric rolls and roll speeds and nonisothermal systems attracted much attention without much progress until recently despite their practical importance. Takserman-Krozer, et al.[10] treated the asymmetrical problem of Newtonian fluid analytically by using the bipolar cylindrical coordinates.

Kiparissides and Vlachopoulous[11] studied the viscous heating effect of the power-law fluid in the symmetric calenders by using the finite element method.

Following the earlier work[12], the study is extended to the problems of viscoelastic fluid flow between asymmetric calender rolls which rotate at different roll speeds. The asymmetry and the nonisothermal effect due to the viscous dissipation incorporated with the Jaumann-Maxwell fluid[13] by the use of the finite difference method and the bipolar cylindrical coordinates. Parameters are investigated through the calculations of the pressure distribution and the power consumption for the optimum operating conditions. The effect of relaxation time of the fluid on the power requirement is also examined in terms of the Weissenberg number.

MATHEMATICAL MODEL AND GOVERNING EQUATIONS

We considered an incompressible linear viscoelastic fluid flow between the asymmetric calenders with unequal diameters and/or different rotating speeds as illustrated in Fig 1. The fluid in calendering is highly viscous so that the inertia force becomes negligibly

** To whom correspondence should be directed.

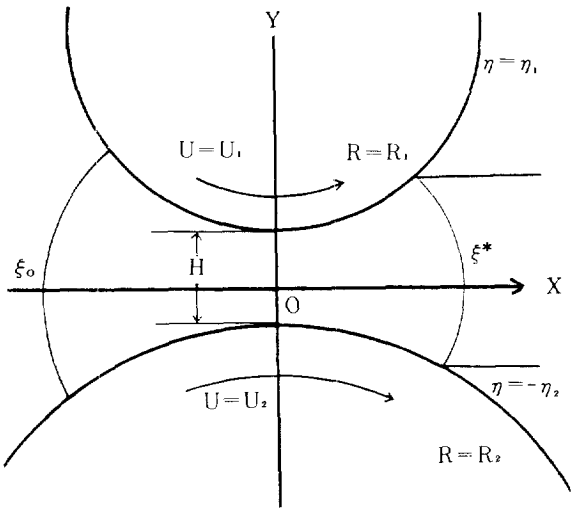

Fig. 1. Asymmetric calender roll geometry.

small. It is also assumed that the rollers are completely rigid and the nip distance is very small compared with the length of other geometric parameters of calenders. For sufficiently small nip distance, the metric tensor of the bipolar coordinate can be approximated as

$$h=\frac{a}{1-\cos\xi} \tag{1}$$

and h becomes a function of ξ only. Applying the above assumptions and also lubrication approximation, the governing equations are given as follows.

Continuity
$$\frac{\partial}{\partial\xi}(hu)+\frac{\partial}{\partial\eta}(hv)=0 \tag{2}$$

Momentum
$$\frac{\partial P}{\partial\xi}=\frac{\partial\tau_{\xi\eta}}{\partial\eta} \tag{3}$$

$$\frac{\partial P}{\partial\eta}=0 \tag{4}$$

Energy
$$\rho C_P\left(\frac{u}{h}\frac{\partial T}{\partial\xi}+\frac{v}{h}\frac{\partial T}{\partial\eta}\right)=\frac{k}{h^2}\left(\frac{\partial^2T}{\partial\xi^2}+\frac{\partial^2T}{\partial\eta^2}\right)+\tau_{\xi\eta}\frac{\partial}{\partial\eta}\left(\frac{u}{h}\right) \tag{5}$$

When a linear viscoelastic fluid model is applied to a large displacement problem, the corotating frame is more appropriate than the material frame. The constitutive equation for the Jaumann-Maxwell fluid is approximately given as

$$\tau_{\xi\eta}+\frac{\lambda}{2}\frac{\partial}{\partial\eta}\left(\frac{u}{h}\right)(\tau_{\xi\xi}-\tau_{\eta\eta})=-\mu\frac{\partial}{\partial\eta}\left(\frac{u}{h}\right) \tag{6}$$

$$\tau_{\xi\xi}=-\lambda\left\{\frac{\partial}{\partial\eta}\left(\frac{u}{h}\right)\right\}\tau_{\xi\eta} \tag{7}$$

$$\tau_{\xi\eta}=\lambda\left\{\frac{\partial}{\partial\eta}\left(\frac{u}{h}\right)\right\}\tau_{\xi\eta} \tag{8}$$

Substituting equations (7) and (8) into equation (6) results in

$$\tau_{\xi\eta}=-\mu\left\{\frac{\partial}{\partial\eta}\left(\frac{u}{h}\right)\right\}/\left[1+\lambda^2\left\{\frac{\partial}{\partial\eta}\left(\frac{u}{h}\right)\right\}^2\right] \tag{9}$$

Boundary conditions on the roll surfaces and at the inlet and outlet must be specified, in addition to the initial distribution for the temperature. We assumed that the calender gap is initially filled with an incompressible fluid whose temperature is the same as that of the feed stream. Thus

$$T=T_0 \quad \text{for } \xi^*\le\xi\le\xi_0,\ -\eta_2\le\eta\le\eta_1 \tag{10}$$

With constant temperature and no slip condition on each roll surface, the boundary conditions are

$$u=U_1,\ T=T_1 \quad \text{at } \eta=\eta_1 \tag{11}$$

$$u=U_2,\ T=T_2 \quad \text{at } \eta=-\eta_2 \tag{12}$$

$$v=0 \quad \text{at } \eta=\eta_1 \text{ and } \eta=-\eta_2 \tag{13}$$

To find the relationship between the entrance coordinate ξ_0 and the exit coordinate ξ^*, it is assumed that when the fluid enters and leaves the deformation zone, the pressure is equal to zero and the pressure gradient at the exit coordinate equals zero such that

$$P=0 \quad \text{at } \xi=\xi_0 \tag{14}$$

$$P=\frac{\partial P}{\partial\xi}=0 \quad \text{at } \xi=\xi^* \tag{15}$$

ANALYTICAL SOLUTION FOR THE ISOTHERMAL SYSTEM

1. Velocity and pressure distribution

With lubrication approximation, the pressure gradient becomes independent of the coordinate η as shown in equations (3) and (4). Upon integrating equation (3) with respect to η after equation (9) is substituted into equation (3), we find the nonlinear differential equation of the form

$$\frac{\partial}{\partial\eta}\left(\frac{u}{h}\right)=\left(\frac{-1}{\mu}\frac{\partial P}{\partial\xi}\eta+C_1\right)\left[1+\lambda^2\left\{\frac{\partial}{\partial\eta}\left(\frac{u}{h}\right)\right\}^2\right] \tag{16}$$

The above equation can be simplified when $\lambda\frac{\partial}{\partial\eta}\left(\frac{u}{h}\right)\ll 1$ as follows.

$$\frac{\partial}{\partial\eta}\left(\frac{u}{h}\right)=\left(-\frac{1}{\mu}\frac{\partial P}{\partial\xi}\eta+C_1\right)+\lambda^2\left(-\frac{1}{\mu}\frac{\partial P}{\partial\xi}\eta+C_1\right)^3 \tag{17}$$

Integrating the equation (17) with respect to η gives the velocity profile such that

$$u=h\left[-\frac{1}{2\mu}\frac{\partial P}{\partial\xi}\eta+C_1\eta-\frac{\mu\lambda^2}{4}\left(\frac{\partial P}{\partial\xi}\right)^{-1}\left(-\frac{1}{\mu}\frac{\partial P}{\partial\xi}\eta+C_1\right)^4+C_2\right] \tag{18}$$

Integration of the equation of continuity with the boundary condition (13) from- η_2 to η_1 gives

$$\int_{-\eta_2}^{\eta_1} \frac{\partial}{\partial \xi}(hu)\, d\eta = 0 \qquad (19)$$

Hence the volumetric flow rate per unit width through the rolls at the steady state is written as the integral form

$$Q = \int_{-\eta_2}^{\eta_1} (hu)\, d\eta \qquad (20)$$

At the exit coordinate ξ^*, Q is expressed by

$$Q^* = (\eta_1 + \eta_2) h^* (U_1 + U_2)/2 \qquad (21)$$

The nonlinear algebraic equations are obtained from the equations (18), (20) and (21) together with the boundary conditions (11) and (12). To determine the three unknowns $\frac{\partial P}{\partial \xi}$, C_1 and C_2, the Newton-Raphson method is used.

The initial trial values for the three unknowns are chosen as those for the Newtonian fluid, which is analytically obtained under the isothermal condition. The relative tolerance for convergence limit for each unknown was taken as 10^{-5}.

The shear stress and normal stress distributions are calculated. The velocity component in η direction is obtained from the equation of continuity. The pressure profile along the passage of the fluid is obtained by integrating the pressure gradient at each cross section by means of trapezoidal rule.

$$P = \int_{\xi^*}^{\xi} \frac{\partial P}{\partial \xi}\, d\xi \qquad (22)$$

The entrance coordinate ξ_0 is calculated from the equation (22) in which the pressure equals the ambient pressure. It represents the minimum bank region to produce a certain film thickness for the given operation conditions, depending on the geometric, kinematic and rheological parameters.

2. Power consumption and roll separating force

The dissipated power in the flow field between two rotating rolls is generally expressed as [10,16]

$$W = \int_{\xi^*}^{\xi_0} \int_{-\eta_2}^{\eta_1} \sum_i \sum_m \tau_{im}\, \dot{\gamma}_{mi}\, h^2 d\eta d\xi \qquad (23)$$

The power requirement per unit volumetric flow rate is obtained by E = W/Q which is an important characteristic of the calendering process, since it stands for the specific energy requirement of the process.

In practice, the film thickness produced is controlled by the geometry of the calenders, especially by the nip distance. The roll separation caused by the stress acting on the roll surfaces in the normal direction must be adjusted by the loading force in order to balance the reactive force of the calendered fluid. This roll separating force per unit width is expressed for the Maxwell fluid by

$$F = \int_{\xi^*}^{\xi_0} h(-p + \tau_{\eta\eta})\, d\xi \qquad (24)$$

FINITE DIFFERENCE METHOD FOR THE NONISOTHERMAL SYSTEM

A finite difference approximation of the energy equation of elliptic type at the steady state with the viscous dissipation term is involved in this study. A two dimensional network in the deformation region is constructed by 81 x 41 mesh system, which is uniform with respect to each of the coordinate, ξ and η. In this problem, the power-law weighted upwind difference scheme[14] is utilized to overcome the numerical instability of the central difference scheme when the grid Peclet number is larger than 4. This numerical scheme is the modified form of the upwind scheme in that the diffusion term is multiplied by the correction factor A (|Pe|),

$$A(|Pe|) = \mathrm{Max}\{0, (1 - 0.1|Pe|)^5\} \qquad (25)$$

where Pe is the grid Peclet number.

From the known velocity profiles and the initial temperature distribution, the temperature field at the next iteration step is computed. This iteration is continued until a certain convergence criterion is satisfied. The convergence criterion of the relative temperature was taken as 10^{-4}. Once the temperature convergence was obtained, new field values of the viscosity and the relaxation time were calculated. The calender gap is so small that it is meaningless to calculate the viscosity field at each grid point. For this reason, the viscosity field is treated from the macroscopic point of view, e.g., mean effective viscosity corresponding to the average temperature at each cross section. The definition of the average temperature is given as follows.

$$T_{av} = \int_{-\eta_2}^{\eta_1} (huT)\, d\eta \Big/ \int_{-\eta_2}^{\eta_1} (hu)\, d\eta \qquad (26)$$

The relationship between the rheological properties and temperature can be expressed as

$$\mu = \mu_o \exp(-\Delta E_1/RT_{av})$$
$$G = G_0 \rho T_{av} \qquad (27)$$

Thus, the change in these rheological properties due to the variation in the temperature distribution results in the improved pressure and velocity distributions. The whole procedure is repeated until the desired accuracy is achieved, which provides the temperature, velocity and pressure distributions at the steady state.

RESULTS AND DISCUSSION

The asymmetric calendering with unequal diameters and different rotating speeds showed quite different results in the pressure distributions compared with the

symmetric cases. It is interesting to note that for the same rotating speeds, the pressure profile becomes maximum as presented in Fig 2 and when the rotaing speed ratio is far from unity the pressure profile decreases. For the Maxwell fluid which has the effect of the shear dependent viscosity expressed as $\mu/[1+\lambda^2\{\frac{\partial}{\partial\eta}(\frac{u}{h})\}^2]$,

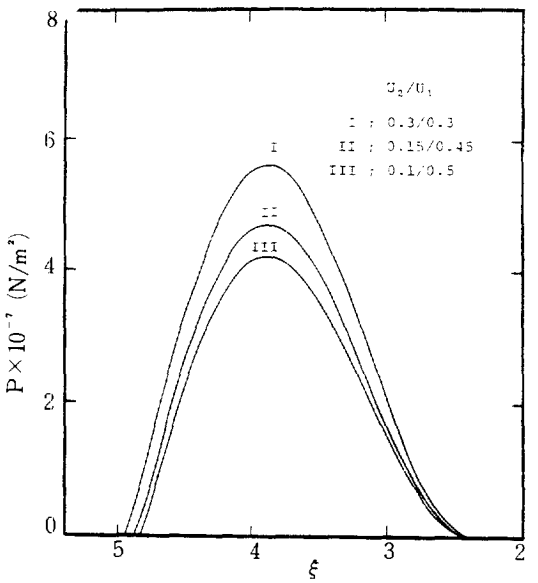

Fig. 2. Pressure profile for different roll speed ratio; $R_1/R_2=0.3/0.3$, $H=0.0001$m, $\xi^*=2.395$, $\mu=400$Pa. s, $\lambda=10^{-4}$ sec.

a speed difference between the rollers induces a distorted velocity profile with larger shear rate. The decreasing pressure is attributed to the corresponding drop in the apparent viscosity. The pressure obviously increases as the sum of the roll radii becomes large simply because the resistance for the flow toward the exit goes up as the sum of the roll radii increases. The effect of roll radius ratio on the pressure force has been also examined, keeping the sum of the radii constant in order to minimize the effect of the variable cross section. The asymmetry in roll size causes slightly lower pressure force than the case of symmetry because the resistance in the nip is lowered with the increase in the asymmetry as shown in Figure 3. However, the relative reduction in maximum pressure due to the asymmetry in roll size is very small as compared to that due to the asymmetry in roll speed. This is because the shear deformation field is much more affected by the asymmetry in the rotating speeds than in diameters. Figure 4 shows the roll separating force and the power consumption per unit volumetric flow rate for various roll size ratio, keeping the sum of radii constant. The symmetry in roll size causes a little larger shear rate than the case

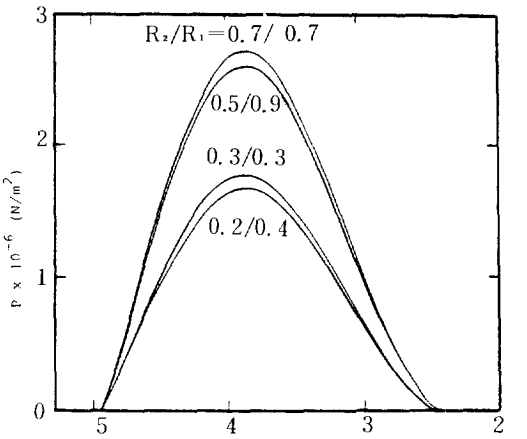

Fig. 3. Pressure profile for various calender geometries; $U_1/U_2=0.3/0.3$, $H=0.001$m, $\xi^*=2.395$, $\mu=400$Pa. s, $\lambda=10^{-3}$ sec.

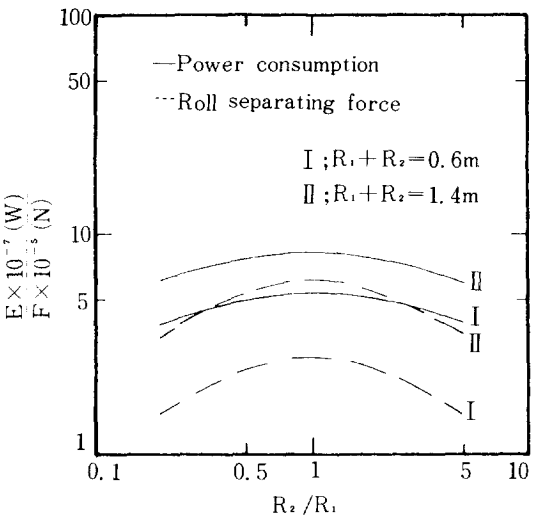

Fig. 4. Power consumption and roll separating force for various roll radius ratios; $U_1/U_2=0.3/0.3$, $H=0.0001$m, $\mu=400$Pa.s, $\lambda=10^{-4}$ sec, $\xi^*=2.395$.

of asymmetry, which brings about the maximum separating force as well as the maximum power consumption. Meanwhile, the change in roll speed ratio with the sum of roll speeds constant shows a somewhat different result. In Fig. 5, the roll separating force attains a maximum when the roll speeds are the same with the same roll size. This fact must be understood in the meaning that the gradient of shear rate is the greatest when the rotating speeds are the same. The power consumption is, however, on the contrary. The larger the asymmetry in the roll speed ratio, the larger the shear deformation

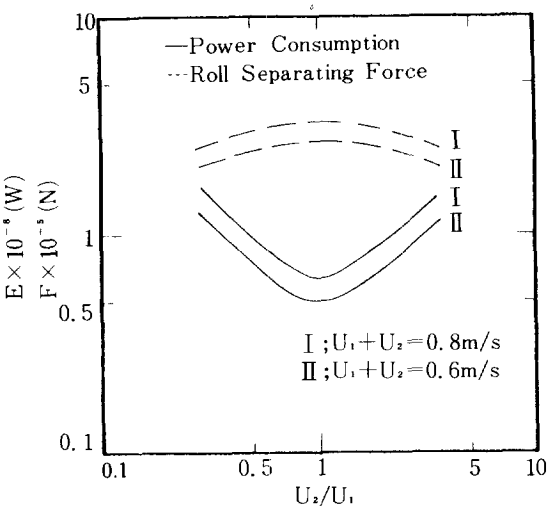

Fig. 5. Power consumption and roll separating force for various roll speed ratios; R_1/R_2 $=0.3/0.3$, $H=0.0001$m, $\xi^*=2.395$, $\mu=400$ Pa. s, $\lambda=10^{-4}$ sec.

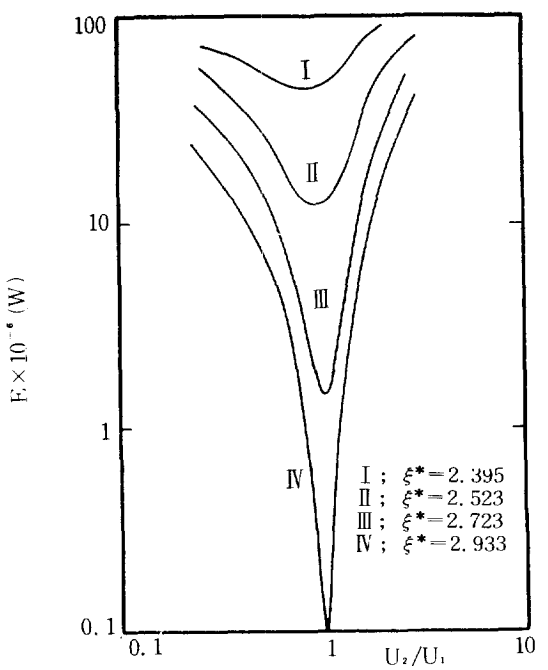

Fig. 6. Relationship between power consumption per unit volume flow rate E and roll speed ratio; $U_1=0.3$m/s, $R_1/R_2=0.4/0.2$, $H=0.0001$m, $\mu=400$Pa. s, $\lambda=10^{-4}$ sec.

becomes, and the less the power consumption at the same roll speeds. Figure 6 reveals that the effect of roll

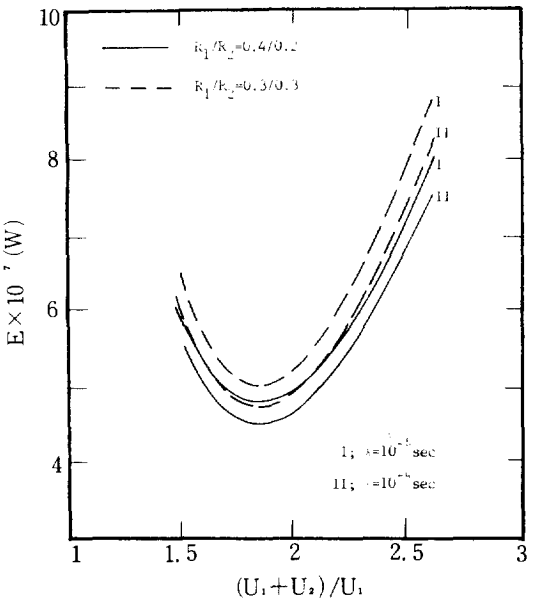

Fig. 7. Power consumption per unit volumetric flow rate for various relaxation times of fluids; $U_1=0.3$m/s, $H=0.0001$m, $\xi^*=2.395$, $\mu=400$Pa. s.

speed ratio on the power consumption E becomes larger as the film thickness decreases and a minimum power consumption per unit volumetric flow rate exists for different roll speeds in the case of realistic condition of film separation. It appears more advantageous when U_2/U_1 is slightly smaller than unity accordingly, with U_1 fixed, as in Figure 6. The relationship between the power consumption E and the roll speed ratio for various relaxation times of fluids and for the same/different roll sizes is shown in Fig. 7. As the relaxation time or the Weissenberg number increases, which corresponds to increase in stiffness of the material, the power consumption decreases for the geometric conditions of interest. This can be explained by the reduction in the shear rate due to the increase in the fluid elasticity.

For the nonisothermal conditions, the temperature rise mainly caused by the viscous heating and also by convection and conduction leads to the reduction in the apparent viscosity and in the shear modulus. The difference between the isothermal and nonisothermal pressure profiles are illustrated in Fig. 8. It is an interesting fact that the minimum bank region expands for the nonisothermal case under the given processing conditions compared with the isothermal case, bringing about the growth of the entrance zone. From this result, it is observed that a point is eventually reached where the velocity of the fluid is zero, which is called the

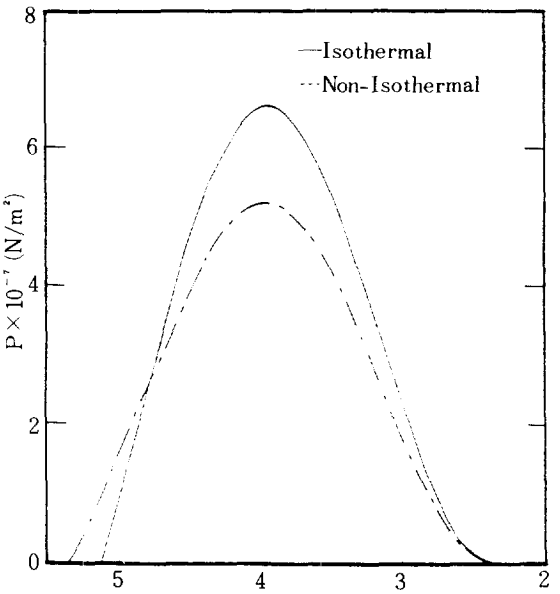

Fig. 8. Comparison of isothermal and non-isothermal pressure profiles; $R_1/R_2=0.1/0.2$, $U_1/U_2=0.3/0.4$, $\xi^*=2.356$, $H=0.0001$m, $T_0=T_2=453°K$, $T_1=443°k$, $K=9.23\times10^{-2}$ W/m°K.

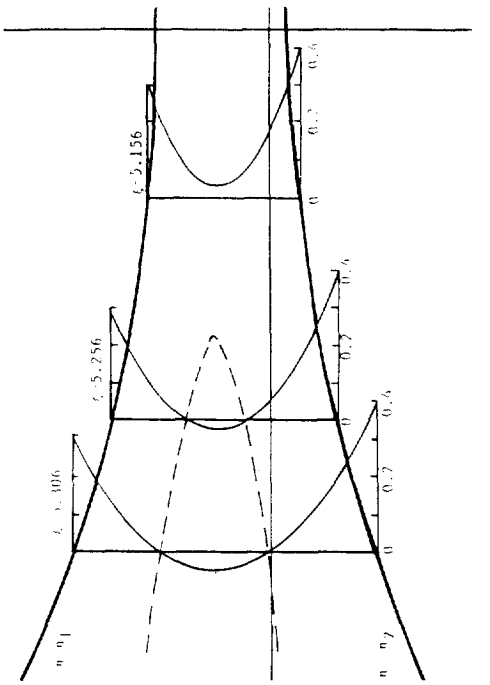

Fig. 9. Stagnation envelope at the entrance coordinate; $R_1/R_2=0.1/0.2$, $U_1/U_2=0.3/0.4$, $\xi^*=2.356$, $H=0.0001$m, $T_0=T_2=453°K$ $T_1=443°K$, $K=9.23\times10^{-2}$ W/m°K.

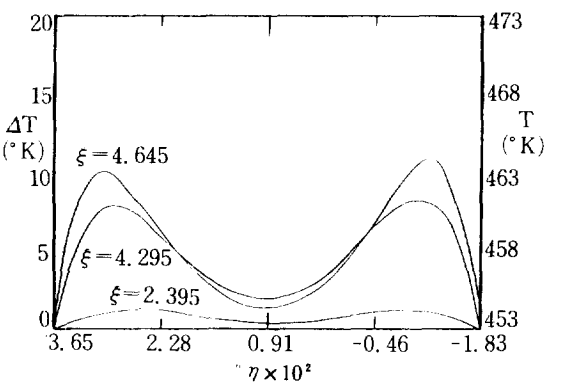

Fig. 10. Temperature distribution at the three different cross-sections; $R_1/R_2=0.1/0.2$, $U_1/U_2=0.3/0.3$, $H=0.0001$m, $\xi^*=2.395$, $T_0=T_1=T_2=453°K$.

stagnation point. Therefore, in the upstream region, there exists the stagnation envelope which clearly confirms the existence of the recirculating flow. The locus of the stagnation envelope is presented by the dashed line as in Fig. 9. The temperature profile developed for the condition of the same rotaing speeds is plotted in Fig. 10. The shear force is greater near the roll surfaces, hence the two maxima are distinctly observed in the vicinity of the roll surfaces in the upstream region. The temperature in the central part of the flow field rises progressively in the further downstream. At the exit plane the maximum is located at about 1/3 of the half gap width from the wall. It is also noted that the value of maximum temperature rises steeply in the inlet region, and drops steadily down to the region of $(2\pi-\xi^*)$. Then it rises again slightly near the nip and drops at the exit as illustrated in Fig. 11. The existence of the two maxima along the flow direction observed in this study agrees with the results for the power-law fluid flow obtained by Kiparissides and Vlachopoulos [11] and also with Lee's [12] results to the extent of the tendency. Meanwhile, Torner's finite difference solution gave only one maximum along the flow direction. However, a careful examination of the experimental profiles of Petrusanskii, et al.[16] reveals the existence of a weak second maximum along the flow direction, agreeing with the present result. On the other hand, a difference in the roll speed exhibits unusual features in the temperature profiles, compared with the case of the same rotating speeds. When the difference in the roll speeds is larger, the velocity profile is almost linear and the shear becomes greater. Hence the influence of the viscous

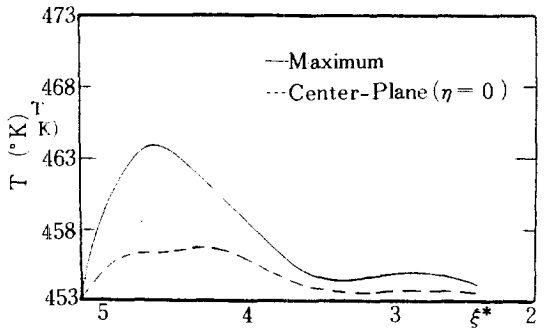

Fig. 11. Maximum and center-plane temperature profiles along the flow direction; R_1/R_2 $=0.1/0.2$, $U_1/U_2=0.3/0.3$, $H=0.0001$ m, $\xi^*=2.395$, $T_0=T_1=T_2=453°K$.

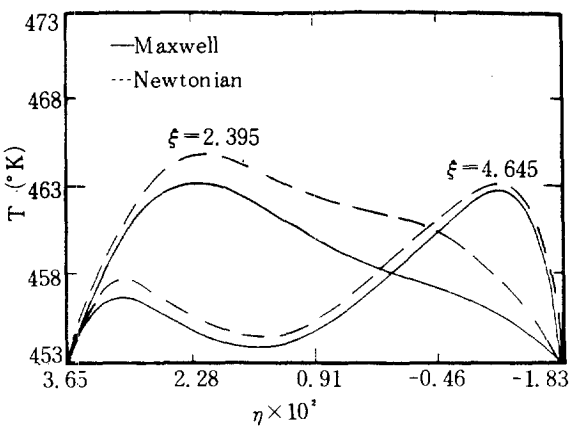

Fig. 12. Temperature distribution at the two different cross-sections; $R_1/R_2=0.1/0.2$, $U_1/U_2=0.2/0.4$, $H=0.0001$m, $\xi^*=2.395$, $T_0=T_1=T_2=453°K$.

heating is severe throughout the whole flow field, not confined to the vicinity of the roll surfaces. The resulting temperature profiles for the Maxwell fluid are compared with those for the Newtonian as an example in Fig. 12. It is interesting to note that in the inlet region the location of a maximum is found near the surface of the fast rotating roll, while at the exit it is shifted to the vicinity of the surface of the slowly rotating roll. As a whole, the temperature profile is higher for the Newtonian fluid than for the Maxwell fluid. This can be explained by the reduction in shear due to the increase in the fluid elasticity. From the results, it may be stated that the asymmetry in roll speeds might play an important role in determining the size and location of the maxima in temperature profiles, which may explain the reason for the occasional appearance of blisters in calendered sheet, as pointed out by Finston.[15]

CONCLUSIONS

1. An analytical solution is obtained for the linear viscoelastic Jaumann-Maxwell fluid flow in the isothermal calendering process. This approximation is valid when the Weissenberg number does not exceed the value of 1.0.
2. The numerical results of this study indicates that the increase in the relaxation time of the fluid leads to the reduction not only in the power requirement but also in the temperature profiles.
3. The maximum temperature profile along the flow direction in the case of the same roll speed has shown two peaks, the first strong and the second weak, as evidenced experimentally.
4. The asymmetry in the roll speeds leads to the higher temperature profile throughout the whole flow field due to the effect of high viscous heating than the symmetric cases in the roll speeds.
5. The effect of roll speed ratio both on the maximum pressure and on the power consumption was significant over the effect of roll size ratio.

Acknowledgement

The authors gratefully acknowledge the Ministry of Education for its 1983 research grants of this study. Parts of the work were presented at the 3rd Pacific Chemical Engineering Congress.

NOMENCLATURE

a :	half distance between the poles (m)
C_1, C_2:	integration constants
C_p:	specific heat of the fluid (J/Kg °K)
E :	power consumption per unit volumetric flow rate (W)
ΔE_1:	activation energy for flow (J/Kg mole °K)
F :	roll separating force (N)
G :	elastic shear modulus (N/m^2)
H :	roll separation at the nip (m)
h :	variable defined by eq. (1) (m)
k :	thermal conductivity (J/m °K)
P :	pressure (N/m^2)
P_e :	grid Peclet number
Q :	volumetric flow rate per unit width (m^3/sec)
Q*:	Q at $\xi = \xi^*$ (m^3/sec)
R_1, R_2 :	radius of upper and lower calendering roll (m)
U_1, U_2:	linear velocity of the calendering rolls, respectively (m/sec)

T: temperature (°K)
T_0, T_1, T_2 : initial fluid temperature and roll surface temperatures, respectively (°K)
u, v: velocity in ξ and η direction, respectively (m/sec)
ξ, η: bipolar cylindrical coordinates
η_1, η_2: values of η at the wall of the rolls
ξ_0, ξ^*: the entrance and the exit coordinates
ρ : fluid density (Kg/m^3)
μ : viscosity of the fluid (Pa. sec)
λ : relaxation time of the fluid (sec)
τ : stress tensor (N/m^2)
$\dot{\gamma}$: rate of deformation tensor (sec^{-1})

REFERENCES

1. Gaskell, R.E.: J. Appl. Mech., **17**, 334 (1950).
2. Bergen, J.R. and Scott, G.W.: J. Appl. Mech., **18**, 101 (1951).
3. Mckelvey, J.M.:"Polymer Processing", John Wiley, N.Y. Ch. 9 (1962).
4. Brasinsky, I. Cosway, H.F. Valle Jr., C.F. Clark Jones, R. and Story, V.: J. Appl. Polymer Sci., **14,** 2771 (1970).
5. Torner, R.V.: "Grundprozesse der Verarbeitung von Polymeren", VEB, Leipzig, E. Germany (1974).
6. Alston Jr., W.W. and Astill, K.N.: J. Appl. Polymer Sci., **17**, 3157 (1973).
7. Paslay, P.R.: J. Appl. Mech., **24**, 602 (1957).
8. Tokita, N. and White, J.L.: J. Appl. Polymer Sci., **11**, 321 (1967).
9. Chong, J.S.: J. Appl. Polymer Sci., **12** 191 (1968).
10. Takserman-Krozer, R. Schenkel, G. rman, G. Rheo. Acta., **14**, 1066 (1975).
11. Kiparissides, C. and Vlachopoulos, J.: Polymer Eng. Sci., **18**, 210 (1978).
12. Lee, Jae Wook and Lee, Ki Jun: J. KIChE, **19,** 303 (1981).
13. Middleman, S.: "Fundamentals of Polymer Processing", McGraw-Hill, New York (1977).
14. Patankar, S.V.: "Numerical Heat Transfer and Fluid Flow", McGraw-Hill, New York, Ch. 5 (1980).
15. Finston, M.: J. Appl. Mech., **18**, 12 (1951).
16. Petrusanskij, J. Yu. and Stachaev, A.I.: Uch. Zap. Jaroslavsk Tech. Inst., t23 (1971).